PERGAMON

Polyhedron 21 (2002) 641–649

POLYHEDRON

www.elsevier.com/locate/poly

Isolated deltahedral clusters of lead in the solid state: synthesis and characterization of Rb_4Pb_9 and $Cs_{10}K_6Pb_{36}$ with Pb_9^{4-}, and $A_3A'Pb_4$ (A = Cs, Rb, K; A′ = Na, Li) with Pb_4^{4-}

Svilen Bobev, Slavi C. Sevov *

Department of Chemistry and Biochemistry, University of Notre Dame, Notre Dame, IN 46556, USA

Received 8 May 2001; accepted 27 November 2001

Abstract

The title compounds were synthesized by direct fusion of the corresponding elements in appropriate atomic ratios at 700 °C, and the structures were determined by single-crystal X-ray diffraction. They contain isolated deltahedral clusters of lead with charge of 4−. The clusters in Rb_4Pb_9 and $Cs_{10}K_6Pb_{36}$ are Pb_9^{4-}. They are *nido* according to their charge, but their shapes do not always correspond to the classical *nido* geometry, a monocapped square antiprism. Some are differently distorted tricapped trigonal prisms. The relationship between these different geometries is discussed, and new classification for such clusters is proposed. The $A_3A'Pb_4$ compounds are isostructural and contain isolated tetrahedra of Pb_4^{4-}.

Keywords: Clusters; Crystal structures; Intermetallic compounds; Lead; Zintl phases

1. Introduction

The growing tendency for miniaturizing semiconducting devices has developed, in recent years, into research on synthesis, characterization and properties of 'quantum-size' particles, i.e. small enough particles that exhibit novel quantum effects [1,2]. Such nanoparticles consist of anywhere between a few atoms to a few hundred atoms of metals or semiconductors. The limited number of atoms in the particle leads to a physical phenomenon known as 'quantum confinement' where the properties of the system fall into the transition region between bulk material and molecules [3]. This leads to different thermodynamic properties such as melting point, phase transitions, and different electronic and optical behavior [4,5].

Large, negatively-charged deltahedral clusters of main-group elements also belong to this group. Such isolated and naked clusters are usually found in compounds containing alkali metals as countercations [6]. Recently, numbers of such species were discovered in 'neat solids' [6,7]. Many of them were previously characterized only in compounds crystallized from liquid ammonia or ethylenediamine solutions of various precursors [8,9]. Such clusters, when in solutions, can react with other molecules, can form polymers, or can oligomerize into larger nanoparticles. They are also fascinating with the aesthetics of their topologies, and better understanding of their unusual bonding will bring knowledge that is otherwise inaccessible [6].

We have undertaken a systematic and thorough search for homoatomic deltahedral clusters of the heavier elements of the carbon group in the solid state. This has resulted in the discovery of the first large deltahedral cluster of group 14, a monocapped square antiprism of Ge_9^{4-} in the binary solid Cs_4Ge_9 [10]. Similar nine-atom clusters of Si, Sn and Pb were later found in Zintl compounds with general stoichiometries A_4Tt_9 and $A_{12}Tt_{17}$ where A = alkali metal and Tt = Tetrel is an element of group 14 (except carbon) [11–14]. Some of these clusters are identical with the Zintl ions crystallized from solutions, and thus establish the relationship between Zintl phases and Zintl ions [10].

* Corresponding author. Tel.: +1-219-631-5891; fax: +1-219-631-6652.

E-mail address: ssevov@nd.edu (S.C. Sevov).

0277-5387/02/$ - see front matter
PII: S0277-5387(01)01016-6

The exploration for clusters in the solid state was later extended into pseudo-binary systems with two different alkali–metal countercations. This has produced several unprecedented compounds with novel features. For example, the first isolated *arachno*-clusters of group 14, square antiprisms of Sn_8^{6-}, were discovered in two Li-containing Zintl phases with stoichiometry of $A_4Li_2Sn_8$ (A = K, Rb) [15]. Similarly, mixed alkali metals and Ge provide the largest, so far, isolated clusters of group 14, giant truncated tetrahedra of Ge_{12}^{12-} in the compound $RbLi_7Ge_8$ [16]. In addition to these compounds with isolated clusters, extended structures are also feasible. Thus, appropriate mixtures of Na/Rb or Na/Cs with Si, Ge and Sn, yielded the first stoichiometric clathrates of type II, $A_8Na_{16}Si_{136}$ and $A_8Na_{16}Ge_{136}$ (A = Rb, Cs) [17,18], the first intermetallic clathrate–III compound, $Cs_{30}Na_{(1.33x-10)}Sn_{(172-x)}$ [19], and a layered clathrate derivative $A_3Na_{10}Sn_{23}$ (A = K, Rb, Cs) with clathrate-II layers 'stuffed' with the Zintl phase A_4Sn_4 [20]. Here, we report on the extension of these studies into the heaviest homologue of the carbon group, lead, and the interesting cluster chemistry of the systems of mixed alkali metals and lead.

Table 1
Selected data collection and refinement parameters for Rb_4Pb_9, $Cs_{10}K_6Pb_{36}$ and Cs_3NaPb_4

Empirical formula	Rb_4Pb_9	$Cs_{10}K_6Pb_{36}$	Cs_3NaPb_4
Formula weight	2206.59	9022.54	1250.48
Temperature (K)	293(2)	293(2)	293(2)
Wavelength (Å), Mo Kα	0.71073	0.71073	0.71073
Crystal system	monoclinic	triclinic	orthorhombic
Space group	$P2_1/m$	$P\bar{1}$	*Cmcm*
Unit cell dimensions			
a (Å)	9.888(1)	9.843(2)	7.267(1)
b (Å)	13.393(4)	15.155(2)	17.282(1)
c (Å)	16.224(3)	15.289(3)	11.074(1)
α (°)		104.51(2)	
β (°)	102.987(8)	97.63(2)	
γ (°)		99.55(1)	
V (Å^3)	2093.7(8)	2149.8(7)	1390.7(2)
Z	4	1	4
D_{calc} (g cm^{-3})	7.000	6.998	5.972
Absorption coefficient (cm^{-1})	812.91	749.49	559.86
Data/parameters	3860/131	7842/439	703/27
Goodness-of-fit on F^2	1.155	0.999	1.034
R_1/wR_2 [a] [$I>2\sigma_I$] (%)	9.12/23.01	11.81/26.34	4.73/11.77

[a] $R_1 = [\Sigma||F_o|-|F_c||]/\Sigma|F_o|$; $wR_2 = \{[\Sigma w[(F_o)^2-(F_c)^2]^2]/[\Sigma w(F_o^2)^2]\}^{1/2}$; $w = [\sigma^2(F_o)^2+(AP)^2+BP]^{-1}$, where $P = [(F_o)^2+2(F_c)^2]/3$.

2. Experimental

2.1. Synthesis

All manipulations were handled in an inert atmosphere glove box or under vacuum. Mixtures of the elements in appropriate atomic ratios (all from Alfa–Aesar or Acros, > 99.9% pure) were loaded in niobium containers. Details on the procedures and the containers can be found elsewhere [21]. Initially mixtures with compositions $(A_{1-x}A'_x)_4Pb_9$ were heated at 700 °C for 1 week and were then slowly cooled to room temperature at a rate of 3° h^{-1}. Phase analysis of the products was carried out with powder X-ray diffraction (Enraf–Nonius Guinier camera with Cu $K\alpha_1$ radiation). For some of them the results were quite ambiguous, and therefore, more reactions with the same atomic ratios were carried out at different temperature regimes. Nevertheless, this did not improve the phase purity of the products, which often contained traces of elemental lead. Later, reactions were loaded with a slight excess of lead intended to serve as a flux for more facile crystal growth. These were carried out at lower temperatures and for prolonged periods of time of about 4 weeks. They produced crystals of better quality that were suitable for data collection.

2.2. Structure determination

A few crystals of each sample were selected in the glove box, sealed in glass capillaries, checked for singularity on a Enraf–Nonius CAD4 single crystal diffractometer with Mo Kα radiation, and data were collected for the best of them at room temperature ($\omega-2\theta$ scans, $2\theta_{max} = 50°$). The following are more details of the data collections: (a) a quarter of a sphere of data was collected of a black, bar-like crystal of Rb_4Pb_9 with dimensions $0.18 \times 0.12 \times 0.10$ mm; (b) a hemisphere of data was collected of a black, very brittle and irregular crystal of $Cs_{10}K_6Pb_{36}$ with dimensions $0.20 \times 0.12 \times 0.10$ mm; (c) an octant of a sphere of data was collected of a dark, bar-like crystal of Cs_3NaPb_4 with dimensions $0.20 \times 0.10 \times 0.06$ mm. The data were corrected for Lorentz and polarization effects, and for absorption with the aid of the XABS program [22a]. The structures were solved by direct methods and refined by full-matrix least-squares on F^2 using the SHELXTL V5.1 package [22b]. Further details of the data collection and structure refinements are given in Table 1. Cs_3LiPb_4, Rb_3LiPb_4 and K_3LiPb_4 are isostructural with Cs_3NaPb_4, and only their lattice parameters are reported (Table 2). Important Pb–Pb distances for Rb_4Pb_9 and $Cs_{10}K_6Pb_{36}$ are given in Tables 3 and 4, respectively.

Table 2
Lattice parameters for other lead compounds with Pb_4^{4-} tetrahedra [a]

Compound	Space group	a (Å)	b (Å)	c (Å)	V (Å^3)
Cs_3NaPb_4 [b]	*Cmcm*	7.267(1)	17.282(1)	11.074(1)	1390.7(2)
Cs_3LiPb_4	*Cmcm*	7.274(1)	16.74(1)	10.75(1)	1309(2)
Rb_3LiPb_4	*Cmcm*	7.133(1)	16.276(2)	10.534(1)	1223.0(3)
K_3LiPb_4	*Cmcm*	6.932(1)	16.09(1)	10.508(2)	1172(3)

[a] Determined from powder diffraction patterns taken at room temperature on an Enraf–Nonius Guinier camera with vacuum chamber, Cu Kα radiation ($\lambda = 1.540562$ Å) and NBS (NIST) silicon as an internal standard.
[b] Determined from 25 reflections at high θ-angles on a CAD4 single crystal diffractometer.

Table 3
Important distances (Å) within the two Pb_9^{4-} clusters in Rb_4Pb_9

	Cluster A			Cluster B	
Pb1A	Pb2A	3.065(6)	Pb1B	Pb3B	3.067(4)
	Pb4A	3.066(6)		Pb4B	3.094(4)
	Pb3A	3.110(4)		Pb5B	3.126(4)
	Pb5A	3.110(4)		Pb2B	3.165(4)
Pb2A	Pb1A	3.065(6)	Pb2B	Pb1B	3.165(4)
	Pb6A	3.142(4)		Pb7B	3.165(4)
	Pb7A	3.142(4)		Pb5B	3.210(4)
	Pb3A	3.397(4)		Pb6B	3.210(4)
	Pb5A	3.397(4)		Pb3B	3.426(6)
Pb3A	Pb8A	3.101(4)	Pb3B	Pb1B	3.067(4)
	Pb1A	3.110(4)		Pb7B	3.067(4)
	Pb7A	3.142(4)		Pb4B	3.317(5)
	Pb2A	3.397(4)		Pb8B	3.317(5)
	Pb4A	3.533(5)		Pb2B	3.426(6)
Pb4A	Pb1A	3.066(6)	Pb4B	Pb1B	3.094(4)
	Pb8A	3.118(5)		Pb9B	3.108(5)
	Pb9A	3.118(5)		Pb8B	3.119(7)
	Pb3A	3.533(5)		Pb3B	3.317(5)
	Pb5A	3.533(5)		Pb5B	3.866(5)
Pb5A	Pb1A	3.110(4)	Pb5B	Pb9B	3.074(4)
	Pb9A	3.131(7)		Pb6B	3.088(7)
	Pb6A	3.142(4)		Pb1B	3.126(4)
	Pb2A	3.397(4)		Pb2B	3.210(4)
	Pb4A	3.533(5)		Pb4B	3.866(5)
Pb6A	Pb9A	3.059(4)	Pb6B	Pb9B	3.074(4)
	Pb7A	3.111(8)		Pb5B	3.088(7)
	Pb2A	3.142(4)		Pb7B	3.126(4)
	Pb5A	3.142(4)		Pb2B	3.210(4)
	Pb8A	4.370(4)		Pb8B	3.866(5)
Pb7A	Pb8A	3.059(4)	Pb7B	Pb3B	3.067(4)
	Pb6A	3.111(8)		Pb8B	3.094(4)
	Pb2A	3.142(4)		Pb6B	3.126(4)
	Pb3A	3.142(4)		Pb2B	3.165(4)
Pb8A	Pb7A	3.059(4)	Pb8B	Pb7B	3.094(4)
	Pb3A	3.101(4)		Pb9B	3.108(5)
	Pb4A	3.118(5)		Pb4B	3.119(7)
	Pb9A	3.131(7)		Pb3B	3.317(5)
	Pb6A	4.370(4)		Pb6B	3.866(5)
Pb9A	Pb6A	3.059(4)	Pb9B	Pb5B	3.074(4)
	Pb4A	3.111(8)		Pb6B	3.074(4)
	Pb5A	3.131(7)		Pb4B	3.108(5)
	Pb8A	3.131(7)		Pb8B	3.108(5)
Average Pb–Pb distance 3.180 Å			Average Pb–Pb distance 3.158 Å		

Table 4
Important distances (Å) within the four Pb_9^{4-} clusters in $Cs_{10}K_6Pb_{36}$

	Cluster C			Cluster D	
Pb1C	Pb5C	3.05(2)	Pb1D	Pb2D	3.03(2)
	Pb2C	3.08(2)		Pb5D	3.05(2)
	Pb4C	3.14(2)		Pb4D	3.07(2)
	Pb3C	3.14(2)		Pb3D	3.08(2)
Pb2C	Pb1C	3.08(2)	Pb2D	Pb1D	3.03(2)
	Pb7C	3.09(3)		Pb7D	3.11(2)
	Pb6C	3.24(2)		Pb5D	3.17(2)
	Pb5C	3.26(2)		Pb6D	3.24(2)
	Pb3C	3.30(2)		Pb3D	3.34(2)
Pb3C	Pb7C	3.05(3)	Pb3D	Pb1D	3.08(2)
	Pb1C	3.14(2)		Pb7D	3.12(2)
	Pb4C	3.15(2)		Pb8D	3.23(2)
	Pb8C	3.29(2)		Pb4D	3.31(2)
	Pb2C	3.30(2)		Pb2D	3.34(2)
Pb4C	Pb8C	3.06(2)	Pb4D	Pb1D	3.07(2)
	Pb9C	3.12(2)		Pb8D	3.11(2)
	Pb1C	3.14(2)		Pb9D	3.16(2)
	Pb3C	3.15(2)		Pb3D	3.31(2)
	Pb5C	3.95(2)		Pb5D	3.72(2)
Pb5C	Pb1C	3.05(2)	Pb5D	Pb1D	3.05(2)
	Pb6C	3.11(2)		Pb6D	3.11(2)
	Pb9C	3.16(2)		Pb9D	3.11(2)
	Pb2C	3.26(2)		Pb2D	3.17(2)
	Pb4C	3.95(2)		Pb4D	3.72(2)
Pb6C	Pb5C	3.11(2)	Pb6D	Pb9D	3.07(2)
	Pb7C	3.11(2)		Pb7D	3.10(2)
	Pb9C	3.14(2)		Pb5D	3.11(2)
	Pb2C	3.24(2)		Pb2D	3.24(2)
	Pb8C	3.91(2)		Pb8D	4.09(2)
Pb7C	Pb3C	3.05(3)	Pb7D	Pb8D	3.07(2)
	Pb2C	3.09(2)		Pb6D	3.10(2)
	Pb6C	3.11(2)		Pb2D	3.11(2)
	Pb8C	3.12(2)		Pb3D	3.12(2)
Pb8C	Pb4C	3.06(2)	Pb8D	Pb7D	3.07(2)
	Pb7C	3.12(2)		Pb9D	3.09(2)
	Pb9C	3.14(2)		Pb4D	3.11(2)
	Pb3C	3.29(2)		Pb3D	3.23(2)
	Pb6C	3.91(2)		Pb6D	4.09(2)
Pb9C	Pb4C	3.12(2)	Pb9D	Pb6D	3.07(2)
	Pb6C	3.14(2)		Pb8D	3.09(2)
	Pb8C	3.14(2)		Pb5D	3.11(2)
	Pb5C	3.16(2)		Pb4D	3.16(2)
Average Pb–Pb distance 3.14 Å			Average Pb–Pb distance 3.13 Å		
	Cluster E			Cluster F	
Pb1E	Pb5E	3.03(2)	Pb1F	Pb5F	3.06(2)
	Pb3E	3.07(3)		Pb4F	3.08(2)
	Pb4E	3.11(2)		Pb2F	3.16(2)
	Pb2E	3.13(3)		Pb3F	3.18(2)
Pb2E	Pb1E	3.13(3)	Pb2F	Pb6F	3.13(2)
	Pb7E	3.18(2)		Pb7F	3.15(2)
	Pb5E	3.21(2)		Pb1F	3.16(2)
	Pb6E	3.27(2)		Pb5F	3.23(2)
	Pb3E	3.38(2)		Pb3F	3.43(2)
Pb3E	Pb1E	3.07(3)	Pb3F	Pb7F	3.15(2)
	Pb8E	3.14(2)		Pb4F	3.17(2)
	Pb7E	3.15(3)		Pb1F	3.18(2)
	Pb4E	3.28(2)		Pb8F	3.26(2)
	Pb2E	3.38(2)		Pb2F	3.43(2)
Pb4E	Pb8E	3.08(2)	Pb4F	Pb9F	3.07(2)
	Pb9E	3.11(2)		Pb1F	3.08(2)
	Pb1E	3.11(2)		Pb8F	3.14(2)
	Pb3E	3.28(2)		Pb3F	3.17(2)
	Pb5E	3.90(2)		Pb5F	3.70(2)

Table 4
Important distances (Å) within the four Pb_9^{4-} clusters in $Cs_{10}K_6Pb_{36}$

Pb5E	Pb1E	3.03(2)	Pb5F	Pb1F	3.06(2)
	Pb6E	3.07(2)		Pb6F	3.07(2)
	Pb9E	3.07(2)		Pb9F	3.11(2)
	Pb2E	3.21(2)		Pb2F	3.23(2)
	Pb4E	3.90(2)		Pb4F	3.70(2)
Pb6E	Pb5E	3.07(2)	Pb6F	Pb5F	3.07(2)
	Pb7E	3.07(2)		Pb7F	3.07(2)
	Pb9E	3.13(2)		Pb2F	3.13(2)
	Pb2E	3.27(2)		Pb9F	3.13(2)
	Pb8E	3.96(2)		Pb8F	4.08(2)
Pb7E	Pb6E	3.07(2)	Pb7F	Pb8F	3.06(2)
	Pb8E	3.09(2)		Pb6F	3.07(2)
	Pb3E	3.15(3)		Pb2F	3.15(2)
	Pb2E	3.18(2)		Pb3F	3.15(2)
Pb8E	Pb4E	3.08(2)	Pb8F	Pb7F	3.06(2)
	Pb7E	3.09(2)		Pb9F	3.13(2)
	Pb9E	3.10(2)		Pb4F	3.14(2)
	Pb3E	3.14(2)		Pb3F	3.26(2)
	Pb6E	3.96(2)		Pb6F	4.08(2)
Pb9E	Pb5E	3.07(2)	Pb9F	Pb4F	3.07(2)
	Pb8E	3.10(2)		Pb5F	3.11(2)
	Pb4E	3.11(2)		Pb6F	3.13(2)
	Pb6E	3.13(2)		Pb8F	3.13(2)
Average Pb–Pb distance 3.14 Å			Average Pb–Pb distance 3.15 Å		

2.3. Magnetic measurements

The magnetizations of the compounds were measured on a Quantum Design MPMS-SQUID magnetometer at a field of 3 T in the temperature range of 10–300 K. Typically 20–40 mg of sample are packed in a special holder designed for air-sensitive compounds [21]. They all showed temperature-independent and negative magnetizations (-3.0×10^{-4}, -3.7×10^{-4}, and -7.2×10^{-4} emu for 37 mg of Rb_4Pb_9, 24 mg of $Cs_{10}K_6Pb_{36}$, and 33 mg of Cs_3NaPb_4, respectively) consistent with electronically-balanced compounds.

2.4. Electronic structure

Extended-Hückel band and MO calculations were carried out within the tight binding approximation with only the lead atoms included (H_{ii} and ζ_1 for Pb 6s: -15.70 eV and 2.35, for Pb 6p: -8.00 eV and 2.06).

3. Results and discussion

3.1. Rb_4Pb_9

This compound is isostructural with K_4Pb_9 [12]. The structure is built of isolated nine-atom clusters of lead, Pb_9^{4-}, that are surrounded by rubidium cations. There are two different clusters in the structure, clusters **A** and **B** (Fig. 1). The geometry of clusters **A** is clearly close to a monocapped square antiprism (Fig. 1(a)), while that of type **B** is closer to a tricapped trigonal prism with two elongated vertical edges (Fig. 1(b)). The way cluster **A** is shown in Fig. 1(a) is somewhat unconventional since the monocapped square antiprism is shown lying on its side. The square of atoms 2–3–4–5 is capped by 1, while square 6–7–8–9 is open. The distances within the clusters range from 3.059(4) to 3.533(5) Å for **A** and from 3.067(4) to 3.426(6) Å for **B** (Table 4). The rubidium cations cap faces, edges, and vertices with the shortest Rb–Pb distances of 3.68(1) Å. There are some relatively short intercluster contacts of 3.767(5) Å between atoms Pb7A and Pb8A of clusters **A** (Fig. 1), and suggest some intercluster interactions. This distance is even shorter in the isostructural K_4Pb_9,

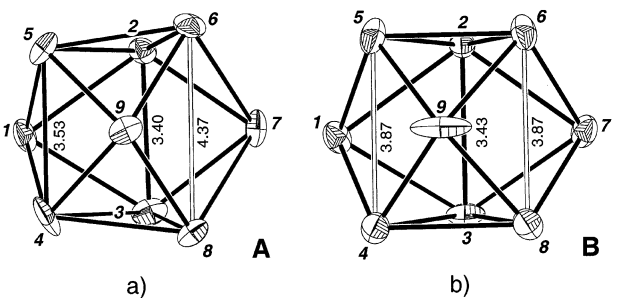

Fig. 1. The two different clusters in Rb_4Pb_9, (a) **A** and (b) **B**. Cluster **A** is a monocapped square antiprisms shown lying on its side (atom 1 caps the square face of atoms 2–3–4–5 while the square face 6–7–8–9 is open). The geometry of cluster **B** is closer to a tricapped (atoms 1, 7, 9) trigonal prism (triangular bases of atoms 2–5–6 and 3–4–8) with two elongated vertical edges (edges 4–5 and 6–8). The thermal ellipsoids are drawn at 50% probability level.

3.669(3) Å, obviously due to the larger size of the rubidium. Nonetheless, it has been proven for the potassium compound that the clusters are not bonded at all [12]. However, the 'short' intercluster contacts affect the density of states by broadening the valence *p*-band more than usual, to a width of about 5 eV. This, in turn, results in a narrow band gap of only about 0.30 eV.

3.2. $Cs_{10}K_6Pb_{36}$

This compound with mixed cations crystallizes in a novel structure type. The triclinic structure (space group *P*1), shown in Fig. 2, contains four crystallographically different clusters of Pb_9^{4-}, labeled **C**, **D**, **E** and **F** (Fig. 3). Interestingly, the corresponding binaries $K_{16}Pb_{36}$ and $Cs_{16}Pb_{36}$ are also known and both contain isolated Pb_9^{4-} [12,13], and yet the mixed cation system provides a new compound with the same overall composition $(Cs_{10}K_6)Pb_{36}$ and the same type of clusters but with a different structure. The shortest intercluster distances in this compound are very similar to those in Rb_4Pb_9, 3.70(2) Å, and similarly are not associated with any intercluster bonding interactions. The clusters are ordered in layers parallel to the (*a*, *b*)-plane (horizontal in Fig. 2). Their positions in each layer correspond to the positions of close-packed spheres, and the layers are stacked on top of each other as in hexagonal close-packed structures, i.e. they follow the order ABAB.

All four clusters in $Cs_{10}K_6Pb_{36}$ have two open square faces (Fig. 3) which clearly excludes classification as monocapped square antiprisms which have only one such face. All four geometries are somewhat closer to tricapped trigonal prisms with two elongated heights.

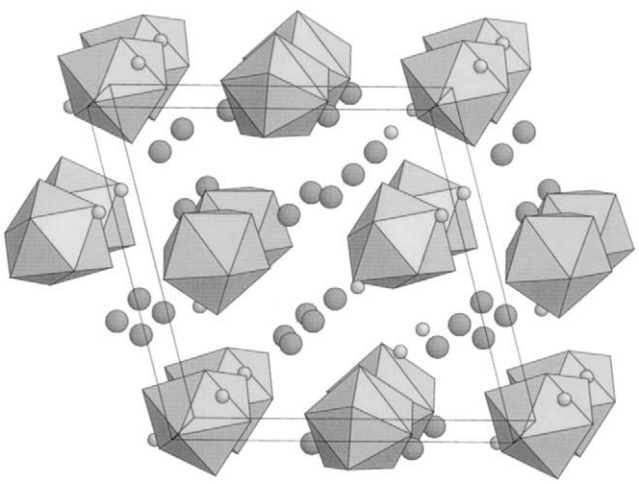

Fig. 2. A polyhedral view of the structure of $Cs_{10}K_6Pb_{36}$ along the *a* axis (*b* is horizontal) with the triclinic cell outlined. The isolated clusters of Pb_9^{4-} form nearly close-packed layers parallel to the (*a*,*b*)-plane, and these layers are stacked in a hexagonal close-packing fashion, i.e. ABAB. There are four clusters per unit cell and all are crystallographically different. The large and small isolated circles are Cs and K, respectively.

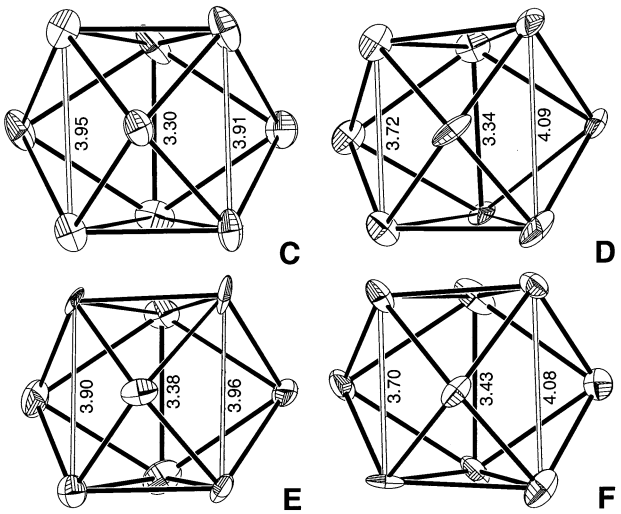

Fig. 3. The four clusters in $Cs_{10}K_6Pb_{36}$ labeled **C**, **D**, **E** and **F**. The atom numbering is the same as in Fig. 1. The thermal ellipsoids are drawn at 50% probability level.

Despite the 'deviations' from the classical *nido* shape, however, each of these clusters carries a charge typical for *nido*-clusters, 4−, according to the formula $Cs_{10}K_6(Pb_9)_4$. Thus, in this compound as well as in Rb_4Pb_9, we find clusters that do not conform to the *nido*-shape but need the same number of electrons for bonding as the *nido*-clusters. This needs more detailed investigation, and this is presented in the following section.

3.3. Nine-atom clusters

There have been quite extensive discussions in the literature about the geometry of nine-atom clusters and their classification into two classes according to their shapes, monocapped square antiprisms or tricapped trigonal prisms (usually elongated), and accordingly into *nido*- or *closo*-types, respectively [23–25]. However, this classification into two very strict classes is quite an ambiguous process since the clusters are almost never perfect, and it is impossible to draw a line between the two geometries. This is usually done based on a multitude of dihedral angles and edge ratios like those presented in Table 5. Thus, it can be seen from this table that the open square face of cluster **A** (face of atoms 6–7–8–9, Fig. 1) is perfectly planar with a 0° dihedral angle and is also nearly rectangular (Table 3) as expected for a monocapped square antiprism. Also typical for that geometry are the dihedral angles of atoms 5–9–4–1 and 2–1–3–7, 32.1(5) and 33.1(5)°, respectively. In the way the cluster is shown in Fig. 1(a), these angles are also dihedral angles within the waist of a trigonal prism of atoms 5–2–6 (upper triangular base) and 4–3–8 (bottom base) that is tricapped by atoms 1, 9, and 7. Thus, the monocapped square antiprism can be viewed as a tricapped trigonal prism

Table 5
Selected edge ratios and dihedral angles in some nine-atom lead clusters [a]

Cluster	Edge ratios		Dihedral angles			Ref.
	(6–8):(2–3)	(4–5):(2–3)	(6–7–8)/(6–8–9)	(5–9–4)/(1–4–5)	(1–2–3)/(2–3–7)	
Pb_9^{3-}	1.057(1)	1.003(1)	14	20	21	[25]
Pb_9^{4-}	1.305(1)	1.024(1)	0.7(4)	28.8(4)	30.5(4)	[23]
Pb_9^{4-}	1.277(2)	1.047(2)	5.3(2)	22.6(2)	30.6(1)	[13]
Pb_9^{4-}	1.283(1)	1.036(1)	0	32.4(4)	32.9(4)	[12]
Pb_9^{4-}	1.128(1)	1.128(1)	13.0(5)	13.0(5)	28.3(4)	[12]
Pb_9^{4-} (A)	1.286(2)	1.040(2)	0	33.1(5)	32.1(5)	[b]
Pb_9^{4-} (B)	1.128(2)	1.128(2)	13.1(5)	13.1(5)	28.4(4)	[b]
Pb_9^{4-} (C)	1.185(9)	1.197(9)	17.3(7)	9.5(6)	25.3(6)	[b]
Pb_9^{4-} (D)	1.225(9)	1.114(7)	11.5(7)	17.0(6)	25.5(6)	[b]
Pb_9^{4-} (E)	1.172(9)	1.154(8)	9.8(6)	12.7(6)	27.0(7)	[b]
Pb_9^{4-} (F)	1.189(9)	1.079(8)	12.2(6)	13.1(5)	24.9(5)	[b]

[a] The numbering system is from Fig. 1.
[b] This work.

with two normal edges, edges 4–5 and 3–2, and one elongated edge, the 8–6 edge. This is also indicated by the ratios between the three edges (Table 5), a number larger than one for the ratio (6–8): (2–3), 1.286(2), and a number close to one for the ratio of (5–4): (2–3), 1.040(2). The geometry with two short and one long edges is typical for a monocapped square antiprism, and is also the reason for the two large and one zero dihedral angles when considered as a tricapped trigonal prism. These dihedral angles and edge ratios of **A** also compare very well with known lead clusters that have already been 'classified' in the class of monocapped square antiprisms (Table 5).

The corresponding dihedral angles and edge ratios look quite different for the remaining five clusters, **B** through **F**. There are two small and one large deltahedral angles as well as two long and one short edges for the trigonal prism. Such clusters would be classified as distorted tricapped trigonal prisms with two elongated edges. A non-distorted prism, i.e. with three normal edges, would be expected to be a *closo*-cluster with a charge of 2− ($2n+2=20$ bonding electrons for a 9-atom cluster) according to Wade's rules [26]. However, obviously this is not the case for these clusters according to the stoichiometry of the compounds for which the clusters carry charges of 4− ($2n+4=22$ bonding electrons). This is also in agreement with the results from the extended-Hückel molecular orbital calculations performed for these clusters which show large HOMO–LUMO gaps of more than 3 eV for a total of 40 electrons (22 bonding electrons and $9\times 2=18$ lone pair electrons on 9 vertices), and correspondingly charges of 4−. Other examples of tricapped trigonal prisms distorted similarly to a different degree also carry $2n+4$ bonding electrons. Such are the cluster of Bi_9^{5+} in $BiBi_9(HfCl_6)_3$ and $Bi_9(Bi_3Cl_{14})$ [27], the heteroatomic clusters $[In_4Bi_5]^{3-}$ in (K-crypt)$_6$[In_4Bi_5]-[In_4Bi_5]·1.5en·0.5tol [28], Sn_9^{4-} in K(K-crown)$_3$[Sn_9]·en [24], and E_9^{3-} for E = Sn or Pb in (K-crypt)$_6E_9E_9$·1.5en·0.5tol where 'crypt' and 'crown' stand for 4,7,13,16,21,24-hexaoxa-1,10-diazabicyclo-[8,8,8]-hexacosane) and 1,4,7,10,13,16-hexaoxacyclooctadecane, respectively [25].

Introduced here is a new approach towards the shapes of the nine-atom deltahedral clusters. It is based on the general overall MO schemes for these clusters. In essence, it abolishes the classification into the two classes of monocapped square antiprisms and tricapped trigonal prisms, and uses only the class of the tricapped trigonal prisms but with different numbers of elongated edges. Shown in Fig. 4(a, b, c, and d) are four tricapped trigonal prisms with zero, one, two and three elongated

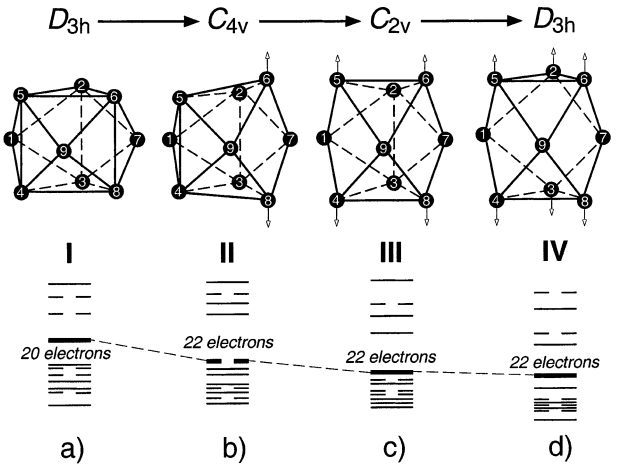

Fig. 4. A schematic representation of the consecutive opening of the three vertical edges of a tricapped trigonal prism (D_{3h}), cluster **I** in (a), along with the corresponding schematic MO diagrams. (b) The elongation of the 6–8 edge leads to a cluster, cluster **II**, with one open square face (C_{4v}) which also happens to be a monocapped square antiprism (shown lying on its side). (c) The elongation of the edge 4–5 of cluster **II** leads to cluster **III** with two open faces (C_{2v}). (d) The elongation of the edge 2–3 of cluster **III** results in an elongated tricapped trigonal prism, cluster **IV**, with three open faces (D_{3h}).

edges, respectively, and the corresponding schematic molecular orbital diagrams. Cluster **I** (Fig. 4(a)) is an ideal tricapped trigonal prism with D_{3h} symmetry and 'normal' (bonding) vertical edges (can be called 'three short' referring to the three vertical edges). The HOMO here is at $2n+2=20$ skeletal electrons but for this particular geometry there is also a relatively large gap above the LUMO a_2'' (shown with a thicker line). This would make the LUMO quite 'attractive' for additional electrons if lowered only a little more, and this can happen as a result of the distortions described below. This a_2' orbital, as it has been discussed before [29], is bonding within the triangular bases of the trigonal prism, i.e. triangles 2–5–6 and 3–4–8, but is antibonding between them (the capping atoms 1, 7, and 9, do not participate). This particular character of the orbital makes it very sensitive to changes in the heights of the prism, and this, combined with its position in the middle of a big gap (Fig. 4(a)), makes it the decisive orbital for the electron count of the cluster.

The cluster shown in Fig. 4(b), cluster **II**, is derived from cluster **I** by elongation of one vertical edge, the edge 6–8. As a result of just this relatively small distortion, the antibonding interactions in what was a_2' LUMO in cluster **I** are relieved, it drops down in energy, becomes occupied as a result of this, and now it is a part of a doubly degenerate HOMO for $2n+4$ electrons. The degeneracy is the result of the C_{4v} symmetry for this cluster which besides being a tricapped trigonal prism with one elongated edge ('two short and one long'), is also the classical monocapped square antiprism as already discussed above (compare with cluster **A** in Fig. 1(a)). This is also the classical shape for a *nido*-deltahedron, i.e. a deltahedron with one missing vertex and a charge of $4-$.

Elongation of a second edge of cluster **II**, the edge 4–5, leads to cluster **III** (Fig. 4(c)). The net character of the orbital in question is even more bonding since the antibonding interactions are reduced even more due to elongation of two instead of one edges. The HOMO–LUMO gap is still at $2n+4$ since nothing else changes significantly in the MO diagram. This cluster of C_{2v} symmetry has two long and one normal edges ('two long and one short') and, therefore, two open square faces. It resembles clusters **B** through **F** (Figs. 1 and 3). Usually the degree of elongation for each edge in a type **III** cluster with two long edges is smaller than that in a type **II** clusters with only one elongated edge. Thus, the edge 6–8 in cluster **A** (type **II**) is 4.370(4) Å while the two edges 4–5 and 6–8 in cluster **B** (type **III**) are 3.866(5) Å (Fig. 1). The same is true for the two long edges in clusters **C** through **F** which are of type **III**; they are all significantly shorter than 4.370(4) Å (Table 4).

Finally, elongation of the remaining third vertical edge of cluster **III** brings back a cluster of D_{3h} symmetry, cluster **IV** (Fig. 4(d)), which is again a tricapped trigonal prism like cluster **I** but is elongated along the threefold axis. The molecular diagram of this cluster ('three long') does not change much from that of cluster **III** and the HOMO–LUMO gap is at the same position. A well known example of this geometry is Bi_9^{5+} in $Bi[Bi_9](HfCl_6)_3$ with three long edges of 3.737 Å [27a].

As already mentioned above, the discussion of the type of a particular nine-atom cluster is often reduced to its classification as a tricapped trigonal prism or a monocapped square antiprism. Fig. 4 clearly shows that such a classification does not unambiguously define the electronic state of the cluster. Thus, clusters **I** and **IV** are both tricapped trigonal prisms but have different electronic requirements due to the relative position of the a_2' orbital. Clusters **II**, **III**, and **IV**, on the other hand, look quite different but have the same numbers of electrons. A very good illustration of this are the clusters **A** through **F**. Therefore, the usual classification of nine-atom clusters into the two classes is an oversimplification since, after all, the monocapped square antiprism is just one component of the series of distorted tricapped trigonal prisms: that with one elongated edge. Table 5 presents a good example of the difficulties when comparing edge ratios and dihedral angles since there are too many of them per cluster and it is impossible to define a cut-off line between the two categories. It is, perhaps, better to use two much more general categories such as 'normal' tricapped trigonal prism and elongated tricapped trigonal prism since these two shapes encompass all observed shapes and also differ in their electron counts. Ultimately, of course, each particular cluster can be discussed in the context of the particular stoichiometry, possible charges based on it, specifics of the shape, measured physical properties, along with careful consideration of the corresponding molecular orbital diagram.

3.4. $A_3A'Pb_4$

The four compounds Cs_3NaPb_4, Cs_3LiPb_4, Rb_3LiPb_4, and K_3LiPb_4 are isostructural with the known Cs_3LiSi_4 [30], and crystallize in the C-centered centrosymmetric space group *Cmcm*. They contain isolated tetrahedral anions of Pb_4^{4-} isoelectronic with the P_4 molecule. The four alkali metal cations provide the four extra electrons and surround the clusters in a very similar way as in the binary APb ($=A_4Pb_4$). However, the much smaller size of Na and Li and their high polarizing power and high electronegativity provide for different interactions in such compounds. For example, the structure of Cs_3NaPb_4 can also be viewed as made of isolated polymeric chains of $_\infty^1[Na(Pb)_4]^{3-}$ (Fig. 5)

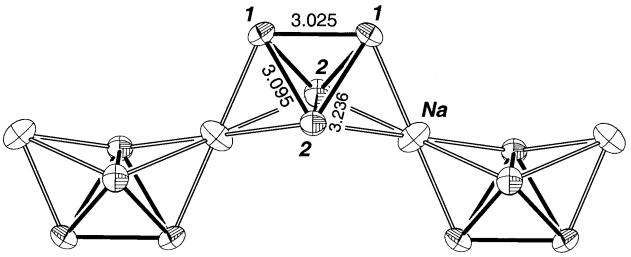

Fig. 5. The isolated polymeric chains of $_{\infty}^{1}[Na(Pb)_4]^{3-}$ running parallel to the c axis in the structure of the mixed-cation compound Cs_3NaPb_4. Lead and sodium are shown as full and crossed ellipsoids, respectively. All thermal ellipsoids are drawn at 80% probability level.

where the sodium cations act as μ_3-ligands coordinated to the staggered faces of two Pb_4^{4-} tetrahedra. The large alkali–metal cations, on the other hand, provide more complete charge transfer and simply separate and screen the chains from each other. Good evidence for the degree of covalency of the Na–Pb interactions is provided by the very different distances in the Pb_4^{4-} cluster. Thus, the edges coordinated to sodium, 1–2 and 2–2, are distinctly longer with distances of 3.095(2) and 3.236(3) Å, respectively, than the edge that is not, 1–1 with a distance of 3.025(2) Å. Furthermore, the edge that is coordinated to two sodium atoms is quite longer than the edges that are coordinated to only one such atom. Semi-covalent interactions of sodium and lithium are quite extensive in other known compounds. It should be pointed out that the 1–1 edge is not completely noncoordinated since it is capped by larger alkali–metal cations, but since the interactions there are almost purely ionic it does not experience elongation. Such combinations of very different alkali metals have been exploited extensively before and account for a large number of novel compounds with unique structures that form only with mixed cations [15–20,31].

4. Conclusions

The isolated nine-atom clusters of lead in the new compounds Rb_4Pb_9 and $Cs_{10}K_6Pb_{36}$ are best described as tricapped trigonal prisms with one or two elongated edges. They carry charges of $4-$, which is consistent with these shapes, and according to the charge they are all *nido* species with $2n+4$ bonding electrons. The commonly used classification of nine-atom clusters into two geometrical classes is not sufficient for accurate description of the electron counts for the clusters.

5. Supplementary material

A combined CIF file for the three structures has been deposited. Further details of the crystal structure determinations can be ordered from Fachinformationszentrum Karlsruhe, D-76344 Eggenstein-Leopoldsshafen, Germany (fax: +49-7247-808-666; e-mail: crysdata@fiz-karlsruhe.de), on quoting the depository CSD-numbers 411891 (Rb_4Pb_9), 411892 ($Cs_{10}K_6Pb_{36}$) and 411893 (Cs_3NaPb_4).

Acknowledgements

We thank the Petroleum Research Fund, administered by the ACS, for the financial support of this research.

References

[1] Special Section in Science, 254 (1991) 1300.
[2] V.L. Colvin, M.C. Schlamp, A.P. Alivisatos, Nature 370 (1994) 354.
[3] L.E. Brus, Appl. Phys. A 53 (1991) 465.
[4] H. Weller, Angew. Chem., Int. Ed. Engl. 32 (1993) 41.
[5] A.P. Alivisatos, Science 271 (1996) 933.
[6] J.D. Corbett, Angew. Chem., Int. Ed. 39 (2000) 670.
[7] The use of 'neat' here (after J.D. Corbett in Ref. [8]) is to distinguish solids made by solid-state reactions from 'molecular' solids crystallized from solution.
[8] J.D. Corbett, Chem. Rev. 85 (1985) 383.
[9] J.D. Corbett, Structure Bonding 87 (1997) 157.
[10] V. Quenéau, S.C. Sevov, Angew. Chem., Int. Ed. Engl. 36 (1997) 1754.
[11] V. Quenéau, E. Todorov, S.C. Sevov, J. Am. Chem. Soc. 120 (1998) 3263.
[12] V. Quenéau, S.C. Sevov, Inorg. Chem. 37 (1998) 1358.
[13] E. Todorov, S.C. Sevov, Inorg. Chem. 37 (1998) 3889.
[14] H.-G. v. Schnering, M. Baitinger, U. Bolle, W. Carrilo-Cabrera, J. Curda, Y. Grin, F. Heinemann, J. Llanos, K. Peters, A. Schmeding, M. Somer, Z. Anorg. Allg. Chem. 623 (1997) 1037.
[15] S. Bobev, S.C. Sevov, Angew. Chem., Int. Ed. 39 (2000) 4108.
[16] S. Bobev, S.C. Sevov, Angew. Chem., Int. Ed. 40 (2001) 1507.
[17] S. Bobev, S.C. Sevov, J. Am. Chem. Soc. 121 (1999) 3795.
[18] S. Bobev, S.C. Sevov, J. Solid State Chem. 153 (2000) 92.
[19] S. Bobev, S.C. Sevov, J. Am. Chem. Soc. 123 (2001) 3389.
[20] S. Bobev, S.C. Sevov, Inorg. Chem. 39 (2000) 5930.
[21] S. Bobev, S.C. Sevov, Inorg. Chem. 38 (1999) 2672.
[22] (a) N. Walker, D. Stuart, Acta Crystallogr., Sect. A 39 (1983) 158; (b) SHELXTL, Version 5.1: Bruker AXS, Madison, WI, 1998.
[23] J. Campbell, D.A. Dixon, H.P.A. Mercier, G.J. Schrobilgen, Inorg. Chem. 34 (1995) 5798.
[24] T.F. Fässler, R. Hoffmann, Angew. Chem., Int. Ed. Engl. 38 (1999) 543.
[25] (a) T.F. Fässler, M. Hunziker, Inorg. Chem. 33 (1994) 5380; (b) T.F. Fässler, M. Hunziker, Z. Anorg. Allg. Chem. 622 (1996) 837.
[26] K. Wade, Adv. Inorg. Chem. Radiochem. 18 (1976) 1.
[27] (a) R.M. Friedman, J.D. Corbett, Inorg. Chem. 12 (1973) 1134; (b) A. Hershaft, J.D. Corbett, Inorg. Chem. 2 (1963) 979.
[28] L. Xu, S.C. Sevov, Inorg. Chem. 39 (2000) 5383.
[29] J.D. Corbett, R.E. Rundle, Inorg. Chem. 3 (1964) 1408.
[30] H.-G. v. Schnering, M. Schwarz, R. Nesper, Angew. Chem., Int. Ed. Engl. 25 (1986) 566.
[31] (a) H.-G. v. Schnering, M. Schwarz, R. Nesper, J. Less-Common Metals 137 (1988) 297; (b) R. Nesper, Angew. Chem., Int. Ed. Engl. 30 (1991) 789 and references therein.